Twenty-Seventh Symposium (International) on Combustion/The Combustion Institute, 1998/pp. 2351–2357

THERMAL DECOMPOSITION OF GASEOUS AMMONIUM DINITRAMIDE AT LOW PRESSURE: KINETIC MODELING OF PRODUCT FORMATION WITH *ab initio* MO/cVRRKM CALCULATIONS

J. PARK, D. CHAKRABORTY AND M. C. LIN

Department of Chemistry
Emory University
Atlanta, GA 30322, USA

The thermal decomposition of ammonium dinitramide, $NH_4N(NO_2)_2$ (ADN), in the gas phase has been studied at 373–920 K by pyrolysis/mass spectrometry under low-pressure conditions using a Saalfeld reactor. The reaction of the sublimed mixture of NH_3 and $HN(NO_2)_2$ (dinitraminic acid, DN) was found to be initiated by the unimolecular decomposition of DN, $HN(NO_2)_2 \rightarrow HNNO_2 + NO_2$, followed by the rapid decomposition reaction, $HNNO_2 + M \rightarrow N_2O + OH + M$. The measured absolute yields of NH_3, H_2O, N_2, and N_2O, calibrated with standard mixtures, could be satisfactorily modeled at 10 Torr He carrier gas pressure by employing the theoretically computed values of $k_2 = 6.79 \times 10^{48}\, T^{-11.0} \exp(-21780/T)$ s^{-1} and $k_3 = 7.53 \times 10^{24}\, T^{-2.9} \exp(-12958/T)$ $cm^3/(mol\ s)$ by high-level *ab initio* molecular orbital and canonical variational Rice-Ramsperger-Kassel-Marcus (MO/cVRRKM) calculations. The key reactions with recommended rate constants are presented.

Introduction

There has been an avalanche of research activity on the kinetics and mechanism of the ammonium dinitramide (ADN) decomposition reaction [1–9] since the earlier studies of Brill, Rossi, and coworkers [1,2]. The majority of these studies focuses on product detection, typically at temperatures above its melting point, 365 ± 1 K, under pressurized conditions where both gaseous and condensed-phase species are involved in the overall decomposition process. The results of these studies, including the latest papers by Oxley [7], Wight [8,9] and their collaborators, reported the observation of rapid production of varying quantities of nitrogen oxides (NO, NO_2, and N_2O) with the apparent activation energy for the overall disappearance of ADN to be in the range of 40–48 kcal/mol.

By T-jump Fourier transform infrared (FTIR) spectroscopy, Brill and coworkers [1] detected the fast appearance of NH_3, N_2O, NO_2, H_2O, and HNO_3 under 1 atm Ar. They proposed the following two branches of global decomposition reactions:

$$ADN(s) \rightarrow NH_3 + HN(NO_2)_2 \qquad (1a)$$

$$\rightarrow NH_3 + N_2O + HNO_3 \qquad (1b)$$

The decomposition of dinitraminic acid (DN) and reactions of its fragments may qualitatively yield from branch (1a) the global product stoichiometry: $9ADN \rightarrow 6\ NH_3 + 7N_2O + 10NO_2 + 9H_2O + 3N_2$ [1].

In a similar qualitative study by Rossi et al. [2], carried out under high-vacuum (10^{-7} Torr) conditions by FTIR spectroscopy for the detection of frozen products on a cold KCl window and by mass spectrometry for the analysis of residual gases, the decomposition of ADN in a Pyrex capillary tube heated to 443 K was found to produce predominantly NH_3, N_2O, NO, H_2O, and a comparable amount of DN.

To elucidate the mechanism of the ADN decomposition reaction, we had earlier investigated the thermochemistry of the system by high-level *ab initio* molecular orbital (MO) calculations [10]. The results of this study led us to the conclusion, similar to that reached by Politzer and coworkers [11,12], that ADN is unstable in ionic form, $NH_4^+ N(NO_2)_2^-$, and its sublimation leads to the formation of two molecular complexes, $H_3N \cdot HN(NO_2)_2$ and $H_3N \cdot HON(O)NNO_2$, which are more stable than the dissociated states, $NH_3 + HN(NO_2)_2$ and $NH_3 + HON(O)NNO_2$, by 12.4 and 14.1 kcal/mol, respectively. The former DN isomer was calculated at the Gaussian-1 (G1) level of theory to have 38.4 kcal/mol dissociation energy producing $NO_2 + HNNO_2$, whereas the latter DN′ isomer has a dissociation energy of 40.1 kcal/mol yielding $NO_2 + HON(O)N$. The overall energy difference for the formation of DN and DN′ from ADN(s) was predicted to be 4.2 kcal/mol, which gives an DN/DN′ isomeric ratio of 3×10^{-3} at the sublimation temperature $T = 362$ K, about 3° below its melting point. Because the DN′ isomer can undergo the isomerization/decomposition reaction producing $HNO_3 + N_2O$ via a

four-centered transition state [10], the apparent enrichment of ADN(s) with AN(s, ammonium nitrate) by the sublimation/decomposition process can be readily understood.

In this study, we focus our kinetic measurements under low-pressure conditions and in the early stages of sample sublimation by pyrolysis/mass spectrometry so as to elucidate the overall gas-phase reaction mechanism:

$$ADN(s) \rightarrow NH_3 + HN(NO_2)_2 \rightarrow \text{products}$$

The rates of formation of the products that can be unambiguously measured and quantitatively calibrated (N_2, N_2O, H_2O, and NH_3) are kinetically modeled. The results of this study, aided by our new high-level *ab initio* MO/statistical-theory calculations for the unimolecular decomposition of DN and $HNNO_2$, are reported here.

Experimental Procedure

The study of the thermal decomposition reaction of sublimed ADN was carried out by using a pyrolysis/mass spectrometric technique in the temperature range 373–920 K. The schematic diagram for the experiment is shown in Fig. 1. The description of the supersonic mass-spectrometric sampling technique, first used by Saalfeld and coworkers [13], has been given elsewhere [14,15]. Only a brief description of the sublimation process will be given here.

The sublimation of ADN took place in a thermostatted sample holder. To achieve homogeneous heating of the sample, we used continuously circulated hot ethylene glycol–water solution using a NESLAB RTC-110 temperature controller that has an accuracy and reproducibility of 0.3 K. The pyrolysis of the sublimed ADN sample entrained with 10 Torr He carrier gas was performed under slow-flow conditions in a Saalfeld-type quartz tubular reactor tube [13], which has an inner diameter of 10 mm and a length of 150 mm with a conical sampling hole at the center. The reactor was mounted perpendicularly to the detection axis of a quadrupole mass spectrometer (QMS, Extrel Model C50), and the reaction tube was wrapped with a 15-mm-thick, 15-mm-wide Nichrome ribbon and insulated with ceramic wool. The reactor temperature could be varied from 300 to 1000 K by adjusting the current through the heater. To minimize heterogeneous surface effects, the inner wall of the reactor was pretreated with boric acid, followed by an extensive bake-out at 1000 K under high vacuum.

The detection chamber housing the mass spectrometer was separated from the supersonic expansion chamber by a metal plate with a 1.0-mm orifice skimmer (Beam Dynamics Model 1) mounted at the center of the plate. The supersonically expanded molecular beam was introduced through the skimmer into the ionization region of the spectrometer. During the experiment, the pressures in the reaction and detection chambers were maintained at (5–10) $\times 10^{-5}$ and (5–10) $\times 10^{-6}$ Torr, respectively.

ADN samples were obtained from the Naval Surface Warfare Center with a purity of 97% to 99% ADN and 3% to 1 % AN (ammonium nitrate); they were used without further purification. NH_3, H_2O (deionized water), and N_2O were purified by standard trap-to-trap distillation. He and N_2 (99.9995%, UHP, Specialty Gases) were used without further purification. After an ADN sample was introduced into the reaction system, it was typically evacuated under high vacuum for several days to minimize water contamination.

The absolute concentrations of NH_3, N_2, N_2O, and H_2O were calibrated with carefully prepared standard mixtures. The initial concentrations of DN, generated by the sublimation of ADN at 362 K, were assumed to be the same as that of NH_3 measured with the reactor temperature set at 373 K, at which no reaction was found to occur.

Results and Discussion

Ab Initio MO/cVRRKM Calculations

Geometries of NO_2, $HNNO_2$, and DN have been optimized at the hybrid density functional B3LYP/6-311G(d,p) level of theory, based on the Becke three-grid integration and exchange functional [16–18] with the correlation functional by Lee et al. [19]. Vibrational frequencies employed to characterize stationary points, zero-point energies (ZPE), and rate constant calculations have also been calculated at this level of theory. To obtain a more accurate description of the reaction path, we used the G2M(RCC,MP2) method of Mebel et al. [20], which approaches high-level results using a series of single-point calculations for basis set size, correlation energy, and systematic error corrections. All calculations were carried out with the Gaussian 94 program [21].

Because the reaction path for the decomposition of DN does not have a well-defined transition state (TS) because of the absence of a reaction barrier, we applied here the canonical variational method based on the evaluation of the maximum free energy of activation ($\Delta G^{\#}$) at each temperature along the reaction path [22–25]. We scanned the potential energy surface for the dissociation of DN to $HNNO_2$ and NO_2 at the B3LYP level. The dissociating N–N bond distance of DN was varied from 1.8 A to 3.0 A with an interval of 0.1 A; other geometric parameters were optimized for each value of the N–N separation. For each structure, we calculated the 3N-7 vibrational frequencies projected out of the gradient direction. This B3LYP calculated energy at each point along the reaction path was used to evaluate

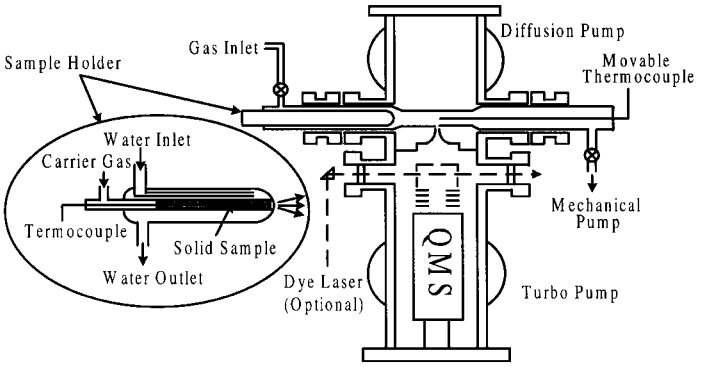

FIG. 1. Schematic diagram of the experimental apparatus.

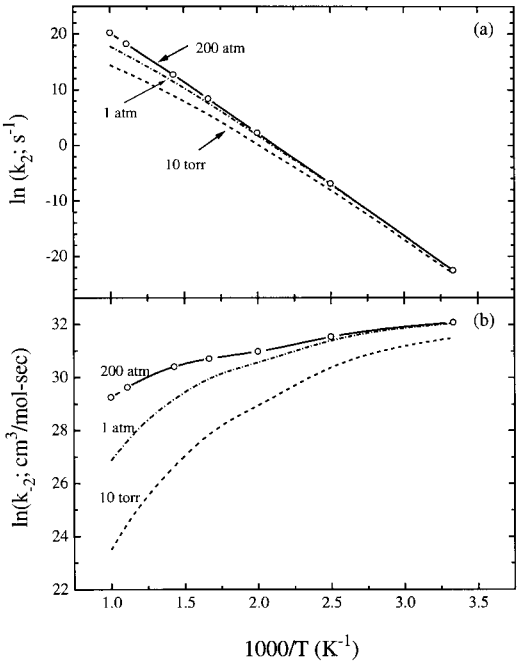

FIG. 2. Arrhenius plots for the DN decomposition (a) and its reverse association (b) reactions.

the Morse potential energy function and then scaled by using the scale factor obtained by comparing N–N dissociation energies at G2M and B3LYP levels. The Morse potential energy was given by the following formula:

$$E(r) = D_e\,[1 - e^{-\beta(R-R_e)}]^2 \qquad \text{(I)}$$

with D_e = 37.9 kcal/mol, R_e = 1.463 Å, and β = 2.42 $Å^{-1}$. The dissociation energy obtained by the G2M method, 37.9 kcal/mol, agrees very well with the G1 calculated value of Mebel et al., 38.4 kcal/mol [10]. The computed moments of inertia, the vibrational frequencies, and the dissociation energy given in the preceding as a function of R were used to search for the maximum Gibbs free energy change ($\Delta G^{\#}$) at various temperatures in the range of 300 to 1000 K. The accurate position of the maximum for each temperature was calculated on the basis of the parabolic fit to the three largest ΔG values. All the molecular parameters corresponding to the structure with a $\Delta G^{\#}$ for each temperature were then used for the RRKM calculation. As the $\Delta G^{\#}$ maxima along the reaction path are located between the calculated structures, the corresponding moments of inertia and vibrational frequencies were obtained by interpolation [23,24]. The high-pressure rate constant for the decomposition of DN is related to $\Delta G^{\#}$ by the well-known equation:

$$k_2^{\infty} = (k_B T/h)\,\exp(-\Delta G^{\#}/RT) \qquad \text{(II)}$$

where k_B is the Boltzmann constant and h the Planck constant [26].

Vibrational modes with frequencies below 50 cm^{-1} were treated as free internal rotations for both DN and the transition state. The calculated decomposition and reverse association rate constants for DN are shown in Fig. 2. Least-squares analysis of rate constants for the decomposition process at the high-pressure limit, 200 atm, 1 atm, and 1.32 × 10^{-2} atm (10 Torr) for He or Ar as diluent can be represented by the following expressions:

$$k_2^{\infty} = 1.92 \times 10^{17}\,\exp(-18300/T)\ s^{-1} \qquad \text{(III)}$$

$$k_2\ (200\ \text{atm}) = 6.88 \times 10^{16} \times \exp(-18330/T)\ s^{-1} \qquad \text{(IV)}$$

$$k_2\ (1\ \text{atm}) = 1.90 \times 10^{41}\,T^{-8.1} \times \exp(-21500/T)\ s^{-1} \qquad \text{(V)}$$

$$k_2\ (10\ \text{torr}) = 6.79 \times 10^{48} T^{-11.0} \times \exp(-21780/T)\ s^{-1} \qquad \text{(VI)}$$

for the temperature range 300–1000 K. Equation VI was used in our kinetic modeling of the experimental data.

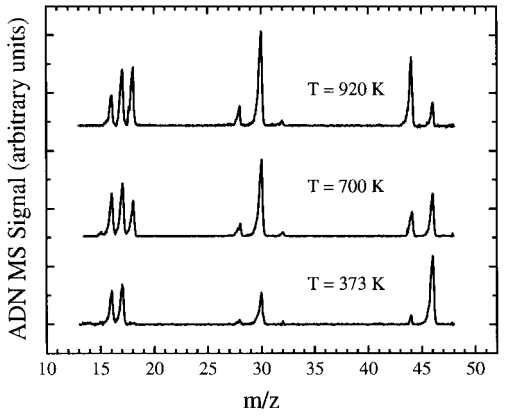

FIG. 3. Mass spectra of the ADN decomposition products at different reaction temperatures as indicated.

Kinetic Modeling of the ADN Decomposition Reaction

Thermal decomposition of ADN, sublimed at the constant temperature of 362 K and carried into a preheated Saalfeld reactor with 10 Torr He carrier gas, was studied in the temperature range 373–920 K. The mass spectra covering m/z = 10–50 obtained at 373, 720, and 920 K reactor temperatures are presented in Fig. 3. No noticeable peaks beyond m/z = 50 were observed within our detectivity. As the reaction does not take place below 450 K in our timescale ($t \leq 40$ ms), the concentration of NH_3 (assumed to be equal to that of DN) and the small concentration of N_2O (Fig. 4, vide infra) were used as the initial concentrations of the reactants present for the kinetic modeling of higher temperature results. Because the DN′ isomer concentration was estimated to be about 0.3% that of DN, its contribution to the formation of various species measured was neglected.

The residence (or reaction) time was calculated with the measured flow rate (F in units of standard cubic centimeter per minute, sccm) based on the ideal gas law, $t(s) = (273 \times 60/760)\,(PV/FT)$, where V is the volume of the reactor in cm^3, P is the total reaction pressure (typically 10 Torr), and T is the reactor temperature.

As indicated, our kinetic modeling was performed with the assumption that $[NH_3]_0 = [DN]_0$ and the reaction were initiated by the unimolecular decomposition of DN followed by the rapid isomerization/dissociation of $HNNO_2$, the nitro-amino radical:

$$HN(NO_2)_2 \rightarrow HNNO_2 + NO_2 \qquad (2)$$

$$HNNO_2 + M \rightarrow N_2O + OH + M \qquad (3)$$

$$HNNO_2 + M \rightarrow NH + NO_2 + M \qquad (4)$$

with $k_3 \gg k_4$, according to the result of our *ab initio* MO/cVRRKM calculations [27]. For kinetic modeling, we employed 152 reactions that have been utilized in our previous studies of the $NH_x + NO_y$ (x = 2,3; y = 1,2) reactions [14,15,28,29] except those involving DN and $HNNO_2$. The key reactions used in the modeling are presented in Table 1.

The results of the modeling, accomplished by using the rate of the initiation reaction 2 computed for the 10 Torr pressure given by equation VI, are presented in Fig. 4 by the solid curves. The agreement

TABLE 1
The key reactions and rate constants[a] for the kinetic modeling of the sublimed ADN system

Reaction	A	n	E_a
1a. $NH_4N(NO_2)_2 = NH_3 + HN(NO_2)_2$		sublimation	
1b. $NH_4N(NO_2)_2 = NH_3 + N_2O + HNO_3$		sublimation	
2. $HN(NO_2)_2 = HNNO_2 + NO_2$	6.79E + 48	−11.0	43277[b]
3. $HNNO_2 + M = N_2O + OH + M$	7.53E + 24	−2.9	25750[c]
4. $HNNO_2 + M = NH + NO_2 + M$	6.35E + 18	−1.1	39397[c]
5. $OH + NH_3 = H_2O + NH_2$	2.00E + 06	2.1	566
6. $OH + OH = H_2O + O$	4.30E + 03	2.7	−2486
7. $HNNO_2 + NO_2 = HNO + NO + NO_2$	3.00E + 12	0	0
8. $HNNO_2 + OH = H_2O + 2NO$	5.00E + 12	0	0
9. $HNNO_2 + OH = HNO + HONO$	5.00E + 12	0	0
10. $NH_2 + NO_2 = H_2NO + NO$	6.56E + 16	−1.5	268
11. $NH_2 + NO_2 = N_2O + H_2O$	1.54E + 16	−1.5	268

[a]Rate constants, defined by $k = AT^n \exp(-E_a/RT)$, are given in units of cm^3, mole, and s; E_a is in units of cal/mol.
[b]First-order rate coefficient for 10 Torr He.
[c]Ref. [24].

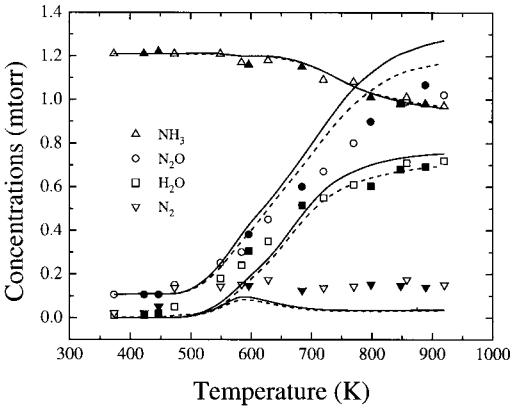

FIG. 4. Comparison of experimental data and kinetic modeling results for the sublimed ADN decomposition process. Filled and open symbols represent experimental data obtained from two different batches of ADN samples. Solid lines are kinetic modeling results with initial concentrations of NH_3 = 1.21 mTorr, $HN(NO_2)_2$ = 1.21 mTorr and N_2O = 0.11 mTorr. Dashed lines are kinetic modeling results with initial concentrations of NH_3 = 1.21 mTorr, $HN(NO_2)_2$ = 1.10 mTorr, N_2O = HNO_3 = 0.11 mTorr. Residence (reaction) time = 19.1/T s (T in Kelvin) and P = 10 Torr with He as carrier gas.

between the modeled concentrations and the measured values is reasonably good, particularly for major products, NH_3, N_2O, and H_2O. The underprediction of N_2, which is a minor product, essentially results from a slight overprediction of N_2O.

Figure 5 presents the results of sensitivity analysis for the three major species measured, NH_3, H_2O, and N_2O at 798 K. Only reactions that are sufficiently influential (3% that of the key process) are included in the figure. The sensitivity coefficient is defined as $S_{ij}(t) = \partial C_i(t)/\partial k_j \times k_j/C_i(t)$, where $C_i(t)$ is the concentration of species i at t and k_j is the rate constant of the jth reaction. As shown in Fig. 5, the OH radical produced by reaction 3:

$$HNNO_2 + M = OH + N_2O + M \quad (3)$$

and removed by reaction 5

$$OH + NH_3 = H_2O + NH_2 \quad (5)$$

is the major reactive species.

In view of the fact that HNO_3 has been shown to be present in the gas phase [1] and in the condensed phase in the form of AN, as already alluded to, in our kinetic modeling we have tested the effect of HNO_3 on the rates of the decay of NH_3 and of the formation of N_2, N_2O, and H_2O. By keeping the initial concentration of NH_3 the same as measured at 373 K reactor temperature, the replacement of 9% DN with HNO_3, based on the initial concentrations of N_2O, led to no noticeable change in the predicted N_2 and NH_3 in our modeling, and only a small decrease (<10%) in N_2O and H_2O yields, resulting primarily from the decrease in the rate of reactions (3). The results of this test are given by dashed curves in Fig. 4. It should be mentioned that the total replacement of DN by HNO_3 resulted in the absence of chemical reaction under the conditions employed.

Key Elementary Reactions

The following elementary reactions play a key role in the decomposition of ADN under low-pressure conditions.

Chain initiation reactions:

$$HN(NO_2)_2 \rightarrow HNNO_2 + NO_2$$

$$HNNO_2 + M \rightarrow OH + N_2O + M$$

Chain propagation reactions:

$$OH + NH_3 \rightarrow H_2O + NH_2$$

$$NH_2 + NO_2 \rightarrow H_2NO + NO$$

$$NH_2 + NO \rightarrow H + N_2 + OH$$

Except for the decomposition of DN and $HNNO_2$, these reactions have been established through our recent studies of the NH_x (x = 2,3) and NO_y (y = 1,2) systems [14,15,28,29]. The rate constant for the DN decomposition (2) has been calculated as described by high-level *ab initio* MO and canonical variational RRKM theories. The predicted value as given in Table 1 was used in the model without adjustment. The rate constant for the decomposition of $HNNO_2$, predicted to be in the second-order region as given in Table 1, was also calculated by c-VRRKM theory based on the potential energy surface computed at the G2M//6-311G(d) level of theory. The detail of the cVRRKM calculation for this reaction will be presented elsewhere [27].

Under high-pressure conditions, the following radical–radical reactions involving $HNNO_2$ are expected to become significant because of the increasing concentrations of radical species:

$$HNNO_2 + OH \rightarrow HNOH + NO_2$$
$$\rightarrow HNO + HONO$$

$$HNNO_2 + NO \rightarrow HNNO + NO_2$$
$$\rightarrow HONO + N_2O$$

$$HNNO_2 + NO_2 \rightarrow HNO + N_2O_3 \text{ (or } NO + NO_2)$$
$$\rightarrow HNO_3 + N_2O$$

Kinetics and mechanisms of these bimolecular nitroamino radical reactions are not known. High-level *ab initio* MO calculations are underway in our laboratory for preparation of the rate constant evaluation.

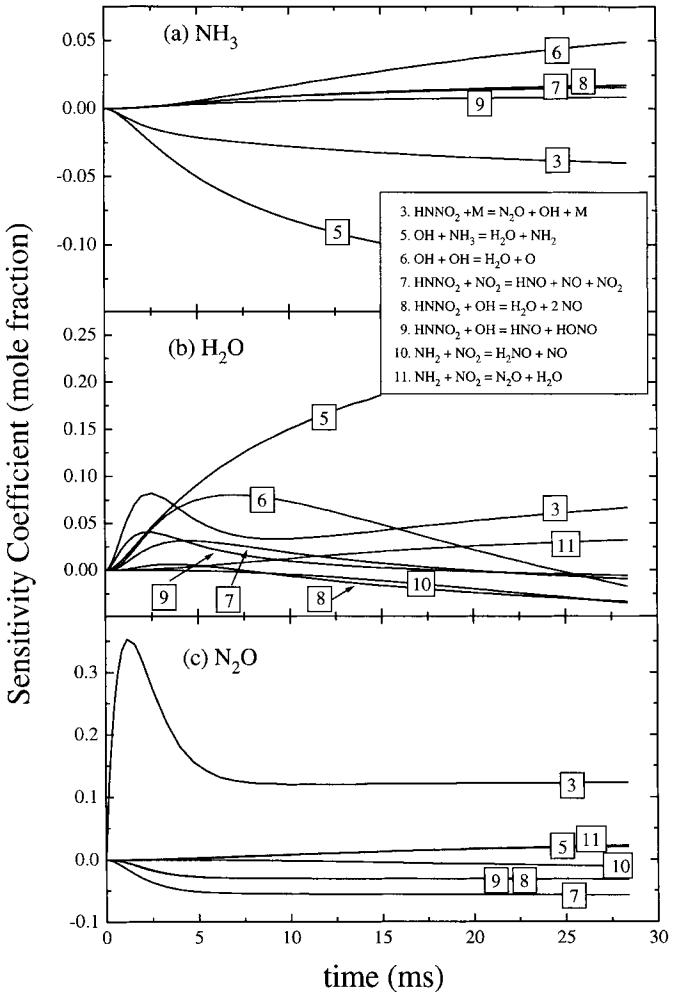

FIG. 5. Sensitivity analysis at 798 K. Conditions: NH_3 = 1.21 mTorr, $HN(NO_2)_2$ = 1.10 mTorr, N_2O = HNO_3 = 0.11 mTorr and P = 10 Torr.

Summary

The absolute yields of N_2, N_2O, H_2O, and NH_3 measured in the thermal decomposition of ADN, sublimed at 3° below melting point, could be satisfactorily accounted for with a mechanism consisting of 152 reactions, assuming that initial concentrations of NH_3 are approximately equal to that of DN. The substitution of 9% DN with HNO_3, which was assumed to have the same concentration as the N_2O detected at reactor temperatures below 450 K (below which no reaction between the reactants was observed), led to a slightly better agreement between experiment and the model.

The mechanism employed was established through our earlier studies of the NH_x (x = 2,3) + NO_y (y = 1,2) systems, with the addition of the reactions involving DN and the nitro-amino ($HNNO_2$) radical whose rate constants were computed theoretically by means of *ab initio* MO/statistical-theory calculations.

Acknowledgments

J. Park and M. C. Lin gratefully acknowledge the support of this work from the Office of Naval Research (contract no. N00014-89-J-1949), and D. Chakraborty is thankful for the support to the Caltech Multidisciplinary University Research Initiative under ONR grant no. N00014-95-1-1388, program managers: Dr. Richard S. Miller and J. Goldwasser. We are also grateful to Drs. A. Stern and S. Caulder of Naval Surface Warfare Center for providing the samples of ADN used in this study.

REFERENCES

1. Brill, T. B., Brush, P. J., and Patil, D. G., *Combust. Flame* 92(1–2):178–186 (1993).
2. Rossi, M. J., Bottaro, J. C., and McMillen, D. F., *Int. J. Chem. Kinet.* 25(7):549–570 (1993).
3. Manelis, G. B., *Int. Annu. Conf. ICT 26th* (Pyrotechnics) 15/1–15/17 (1995).

4. Korobeinichev, O. P., Kuibida, L. V., Paletsky, A. A., and Shmakov, A. G., *Mater. Res. Soc. Symp. Proc.* 418:245–255 (1996).
5. Russell, T. P., Piermarini, G. J., Block, S., and Miller, P. J., *J. Phys. Chem.* 100:3248–3251 (1996).
6. Lobbecke, S., Krause, H. H., and Pfeil, A., *Propellants Explos. Pyrotech.* 22(3):184–188 (1997).
7. Oxley, J. C., Smith, J. L., Zheng, W., Rogers, E., and Coburn, M. D., *J. Phys. Chem. A* 101:5646–5652 (1997).
8. Vyazovkin, S. and Wight, C. A., *J. Phys. Chem. A* 101:5653–5659 (1997).
9. Vyazovkin, S. and Wight, C. A., *J. Phys. Chem. A* 101:7217–7221 (1997).
10. Mebel, A. M., Lin, M. C., Morokuma, K., and Melius, C. F., *J. Phys. Chem.* 99(18):6842–6848 (1995).
11. Politzer, P., Seminario, J. M., and Concha, M. C., *THEOCHEM* 427:123–130 (1998).
12. Politzer, P. and Seminario, J. M., *ACS Symp. Ser.* 677 (Computational Thermochemistry):359–368 (1998).
13. Wyatt, J. R., De Corpo, J. J., McDowell, M. V., and Saalfeld, F. E., *Rev. Sci. Instrum.* 45:916–919 (1974); *J. Mass. Spectrom Ion Phys.* 16:33–38 (1975).
14. Park, J. and Lin, M. C., *J. Phys. Chem. A* 101:5–13 (1997).
15. Park, J. and Lin, M. C., *J. Phys. Chem. A* 101:2643–2647 (1997).
16. Becke, A. D., *J. Chem. Phys.* 96:2155–2160 (1992).
17. Becke, A. D., *J. Chem. Phys.* 97:9173–9117 (1992).
18. Becke, A. D., *J. Chem. Phys.* 98:5648–5652 (1993).
19. Lee, C., Yang, W. and Parr, R. G., *Phys. Rev. B* 37:785–789 (1988).
20. Mebel, A. M., Morokuma, K., and Lin, M. C., *J. Phys. Chem.* 103:7414–7421 (1995).
21. Frisch, M. J., Trucks, G. W., Schlegel, H. B., Gill, P. M. W., Johnson, B. G., Robb, M. A., Cheeseman, J. R., Keith, T., Petersson, G. A., Montgomery, J. A., Raghavachari, K., Al-Laham, M. A., Zakrzewski, V. G., Ortiz, J. V., Foresman, J. B., Cioslowski, J., Stefanov, B. B., Nanayakkara, A., Challacombe, M., Peng, C. Y., Ayala, P. Y., Chen, W., Wong, M. W., Andres, J. L., DeFrees, D. J., Baker, J., Stewart, J. P., Head-Gordon, M., Gonzalez, C., and Pople, J. A. *GAUSSIAN 94, Revision D. 3,* Gaussian, Inc., Pittsburgh, 1995.
22. Garrett, B. C. and Truhlar, D. G., *J. Chem. Phys.* 70:1593–1598 (1979).
23. Hsu, C.-C., Mebel, A. M., and Lin, M. C., *J. Chem. Phys.* 105:2346–2352 (1996).
24. Mebel, A. M., Diau, E. W. G., Lin, M. C., and Morokuma, K., *J. Am. Chem. Soc.* 118:9759–9771 (1996).
25. Madden, L. M., Moskaleva, L. V., Kristyan, S., and Lin, M. C., *J. Phys. Chem. A* 101:6790–6797 (1997).
26. Garrett, B. C. and Truhler, D. G., *J. Chem. Phys.* 70:1595–1598 (1979).
27. Chakraborty, D., Hsu, C.-C., and Lin, M. C., "Theoretical Studies of Nitroamino Radical reactions: Rate Constants for Unimolecular Decomposition of $HNNO_2$ and Related Bimolecular Process," *J. Chem. Phys.*, in press.
28. Thaxton, A. G., Hsu, C.-C., and Lin, M. C., *Int. J. Chem. Kinet.* 29:245–251 (1997).
29. Park, J. and Lin, M. C., *Proc. International Conference on Technologies and Combustion for a Clean Environment,* Lisbon, Portugal, 34.1:1–5 (1997).